REVIEW ARTICLE

Improve the prediction of summer precipitation in the Southeastern China by a hybrid statistical downscaling model

Liu Ying · Fan Ke

Abstract We attempt to apply year-to-year increment prediction to develop an effective statistical downscaling scheme for summer (JJA, June–July–August) rainfall prediction at the station-to-station scale in Southeastern China (SEC). The year-to-year increment in a variable was defined as the difference between the current year and the previous year. This difference is related to the quasi-biennial oscillation in interannual variations in precipitation. Three predictors from observations and six from three general circulation models (GCMs) outputs of the development of a European multi-model ensemble system for seasonal to interannual prediction (DEMETER) project were used to establish this downscaling model. The independent sample test and the cross-validation test show that the downscaling scheme yields better predicted skill for summer precipitation at most stations over SEC than the original DEMETER GCM outputs, with greater temporal correlation coefficients and spatial anomaly correlation coefficients, as well as lower root-mean-square errors.

L. Ying · F. Ke (✉)
Institute of Atmospheric Physics, Chinese Academy of Sciences, Beijing 100029, China
e-mail: fanke@mail.iap.ac.cn

L. Ying
National Climate Center, China Meteorological Administration, Beijing 100081, China

F. Ke
Key Laboratory of Regional Climate-Environment for East Asia, Chinese Academy of Sciences, Beijing 100049, China

1 Introduction

Precipitation over China exhibits complex spatial and temporal structures (Wang and Zhu 2001). Long-term precipitation records show that the interannual variations in China, especially over East China, have a tendency toward a quasi-biennial oscillation: years with above-normal summer rainfall tend to be followed by years with below-normal rainfall and vice versa. This tendency is often referred to as the tropospheric biennial oscillation (the TBO) and is found in the Indian summer monsoon rainfall (Mooley and Parthasarathy 1984; Yasunari 1990; Webster et al. 1998; Meehl and Arblaster 2002). The East Asian monsoon, El Niño-Southern Oscillation (ENSO) and the monsoon rainfall over East China (Li et al. 2001; Meehl 1996; Zhao 1999). Based on the TBO, Fan et al. (2008) proposed a year-to-year increment prediction approach using the difference in a variable between the current year and the previous year as a prediction object. The year-to-year increment approach could facilitate the achieving of amplified predicted skills and adequately produce the interannual and decadal variability of variables. In addition, a year-to-year increment of the variable contains more information on the previous year than it does in the original form, which can improve the prediction quality (Wang et al. 2010). Although the year-to-year increment prediction approach has been applied successfully to seasonal forecasts for area-averaged summer rainfall over the middle-lower reaches of the Yangtze River Valley (Fan et al. 2008) and North China (Fan et al. 2009) as well as for the seasonal prediction of tropical cyclones (Fan and Wang 2009; Fan 2010), it has not been applied to seasonal climate prediction at individual stations in China, though this application would have important practical implications. At present, both dynamical climate models and statistical models have a low predictive capacity for
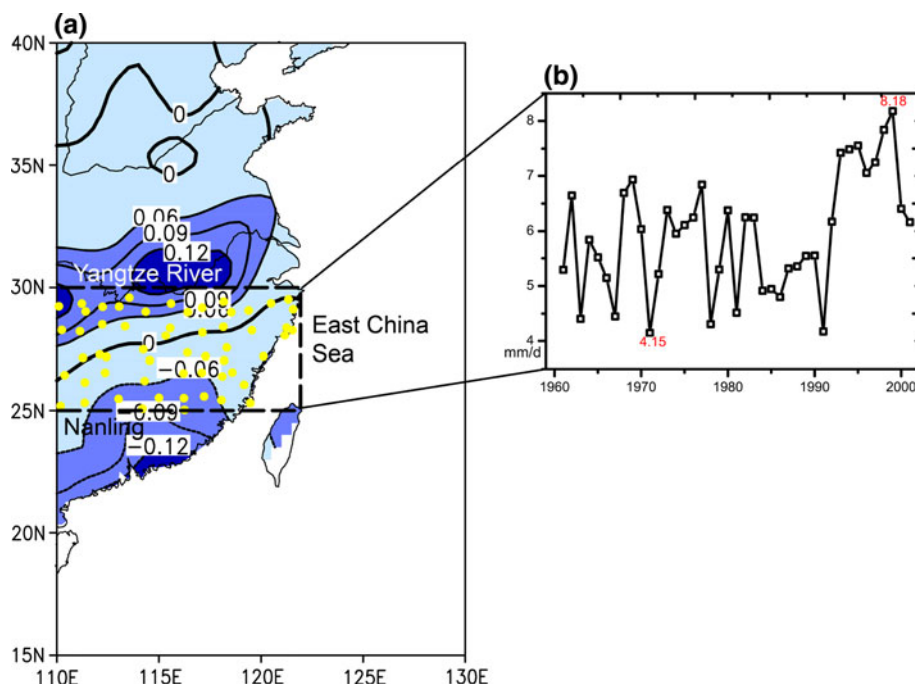
Fig. 1 Geographic location of SEC and the first EOF mode of precipitation over East China (**a**) and the precipitation rate in SEC (**b**) during the summers from 1961–2001. *Shading* denotes the pattern of the first EOF mode, and the *dots* show the locations of 57 stations across SEC

climate prediction when directly applied to given stations (Wang et al. 2008). For this reason, downscaling prediction is proposed. This paper presents the first application of year-to-year increment prediction to summer rainfall in China at the station level.

Southeastern China (SEC) (25°–30°N, 110°–122°E) is the primary agricultural region and the economic and industrial center of China. This region is located south of the Yangtze River, north of Nanling, and west of the East China Sea (Fig. 1a). The first empirical orthogonal function model of summer precipitation over Eastern China illustrates that SEC is an area of transition between the Yangtze River Valley and the region south of Nanling. This region experiences considerable interannual variation, with the maximum and minimum precipitation rates being 8.18 mm/day and 4.15 mm/day, respectively (Fig. 1a, b). The large interannual variations of summer rainfall made it is difficult to be predicted in this region directly by either a dynamical or a statistical model.

In addition, SEC summer rainfall is affected by the East Asian summer monsoon. Usually, a weakened (enhanced) East Asian summer monsoon leads to abundant (deficient) rainfall in SEC, with above (below)-normal water transport via the westward (eastward) movement of the Western North Pacific subtropical high (Chen et al. 2004; Zhou and Yu 2005; Zhao and Zhou 2009). As shown in Table 1, the correlation coefficient between the East Asian summer monsoon index and SEC summer rainfall is 0.47. It is an important and a challenging task to predict station-to-station SEC summer rainfall for either a dynamical climate model or a statistical model.

As predicted, the large-scale atmospheric circulations from the general circulation model (GCM) outputs are generally considered reliable (Gao et al. 2001, 2006, 2012; Wang et al. 2008; Zhou et al. 2009a, b). Especially in tropical regions, it is feasible to identify useful, predictive information from GCMs that can be used to develop effective statistical downscaling predictive models (Wilby and Wigley 1997; Ke et al. 2009; Lang 2011; Lang and Wang 2010; Lang and Zheng 2011; Liu et al. 2011). Unlike these previous works, we not only use the year-to-year increment prediction method but also identify two types of predictors: the predicted summer atmospheric circulation from the global ocean–atmosphere general circulation models hindcasts and preceding atmospheric and ocean observational data, such as the sea-surface temperature (SST) in winter (December–January–February) and the sea-level pressure (SLP) in May. In this way, the hybrid downscaling model can be developed to improve predicted skill for summer rainfall at the station level in SEC. Therefore, the main objective of the current study is using a year-to-year increment downscaling scheme to improve the predicted skill of SEC summer precipitation.

2 Data and methodology

2.1 Data

Global GCM datasets provided by DEMETER (Development of a European multi-model ensemble system for seasonal to interannual prediction) for summers (June–

Table 1 The description of predictors, in which SST_{KU} and SST_{SP} represent the area-averaged SSTs over Kuroshio and the South Pacific Ocean, respectively

Predictors	Period	Datasets	Area-averages	Correlation coefficients
SST_{KU}	1960–2000 winter	HadISST1	20.5°–34.5°N, 120.5°–140.5°E	0.51
SST_{SP}	1960–2000 winter	HadISST1	19.5°–2.5°S, 105.5°–70.5°W	0.59
SLP_{MG}	1961–2001 May	ERA-40	40°–50°N, 90°–110°E	0.57
EAMI	1961–2001 summer	DEMETER	20°–40°N, 110°–125°E	0.47
Z_{200TIB}	1961–2001 summer	DEMETER	25°–35°N, 80°–100°E	−0.38
Z_{500SEC}	1961–2001 summer	DEMETER	20°–30°N, 100°–125°E	0.46
q_{850SIO}	1961–2001 summer	DEMETER	20°–10°S, 70°–100°E	0.31
Div_{200WTP}	1961–2001 summer	DEMETER	10°–20°N, 110°–150°E	−0.68
ζ_{850Pl}	1961–2001 summer	DEMETER	0°–10°N, 110°–130°E	0.52

The correlation coefficients between area-averaged SEC summer rainfall and the predictors during 1961–2001 are shown in the 5th column

SLP_{MG} denotes the area-averaged SLP over Mongolia (40°–50°N, 90°–110°E). *EAMI* East Asian summer monsoon index, Z_{200TIB} denotes the area-averaged Z_{200} over the Tibetan Plateau. Z_{500SEC} denotes the area-averaged Z_{500} over SEC. q_{850SIO} represents the area-averaged q_{850} in the South Indian Ocean. Div_{200WTP} represents the area-averaged 200-hPa divergence in the tropical western Pacific Ocean, and ζ_{850Pl} represents the area-averaged 850-hPa vorticity near the Philippines

July–August) during the period 1960–2001 were used. This system comprises seven global coupled ocean–atmosphere models, which covered different periods, initiated on 1 February, 1 May, 1 August, and 1 November (Palmer et al. 2004), respectively. For the purpose of summer rainfall prediction, datasets with initial conditions starting from 1 May were chosen. Among the seven DEMETER GCMs, three GCMs outputs, i.e., CNRM (Centre National de Recherches Météorologiques, France), ECMWF (European Centre for Medium-Range Weather Forecasts, UK) and UKMO (Met Office, UK), are used in this study. These three DEMETER GCMs have longer hindcast periods than the others, therefore, we can get more extensive period data to establish and validate the downscaling scheme.

The multi-model ensemble (MME) is defined as the average ensemble of these three chosen DEMETER GCMs. Some potential predictors are defined as follows:

East Asian monsoon index (EAMI):

$$EAMI = (u_{850} + v_{850})/2^{1/2}. \tag{1}$$

The EAMI defined by Wang (2000) was used 850-hPa zonal and meridional wind (averaged over 20°–40°N, 110°–125°E). The index is equal in magnitude between the zonal and meridional wind components, and it has been widely used in climate modeling studies (Zhou et al. 2009a).

Wind vorticity at 850-hPa:

$$\zeta_{850} = \frac{\partial v_{850}}{\partial x} - \frac{\partial u_{850}}{\partial y}. \tag{2}$$

Wind divergence at 200-hPa:

$$DIV_{200} = \frac{\partial u_{200}}{\partial x} + \frac{\partial v_{200}}{\partial y}. \tag{3}$$

In addition, ECMWF reanalysis data (ERA-40) are used (Uppala et al. 2005), with a horizontal resolution of 2.5° in latitude and longitude. The monthly SST data are derived from HadISST 1.1 (HadISST1), which is obtained from the Met Office Hadley Centre. These data are composed of a $1° \times 1°$ grid of a global dataset (Rayner et al. 2003). The observed rainfall data at 57 stations over SEC for the period 1960–2001 are obtained from the China Meteorological Administration. The geographical location of SEC in East China and the distribution of the stations are shown in Fig. 1a.

2.2 Methodology

The year-to-year increment of a variable is defined as the difference between the value of the variable in the current year and that in previous year. Based on the variability in the year-to-year increment of summer rainfall at the station level in SEC, a year-to-year increment downscaling model for SEC summer rainfall at a given station is first based on multi-linear regression. Then, the predicted precipitation at the station is calculated as the sum of the predicted year-to-year increments in summer rainfall at this station and the corresponding observed precipitation from the preceding year. In this way, 57 year-to-year increment downscaling prediction schemes for SEC summer rainfall at 57 stations are established. To validate these downscaling predictive models, the spatial anomaly correlation coefficients (ACCs), temporal correlation coefficients (TCCs), root-mean-square error (RMSE) and improved predicted skill (decreased percentage of RMSE) are used. The improved predicted skill is defined as:

$$RMSE_{Per} = (RMSE_{org} - RMSE_{sd})/RMSE_{org} \tag{4}$$

where RMSE$_{org}$ and RMSE$_{sd}$ represents the RMSE of original DEMETER GCMs before and after downscaling, respectively.

3 Predictors

3.1 Large-scale circulation features, 200-hPa geopotential height and 850-hPa vorticity in summer

The predictors are identified from the variables that are closely related to summer rainfall over SEC. First, a composite analysis of the year-to-year increment differences between the years with more and less precipitation in SEC in atmospheric circulation at 200, 500 and 850 hPa is conducted using ERA40 (Fig. 2). The specific more and less precipitation years of SEC is given in Table 2. Corresponding to aberrant rainfall over SEC, an abnormal meridional wind pattern at 200-hPa resembling the '+ − + −' mode appeared over the East Asian coast, extending from Baikal to the Philippines (Fig. 2a). In this pattern, an abnormal anticyclone is observed east of Baikal

Table 2 Selection years of the more and less precipitation in SEC

Summer rainfall	Specific year
More	1968; 1969; 1977; 1993; 1994; 1995; 1996; 1997; 1998; 1999
Less	1963; 1967; 1971; 1978; 1981; 1986; 1991

and the Indo-China Peninsula, and a cyclonic anomaly is found in the Loess Plateau and the Philippines. There is an abnormal cyclone over Tibetan Plateau at 200 hPa, indicating the weakened South Asian High as well as weakened monsoon circulation at high level (Yeh et al. 1979). This phenomenon results in more rainfall over SEC (Chen et al. 2004; Zhao and Zhou 2009). A remarkable localized anticyclone anomaly with divergent airflow over SEC at 200-hPa could yield convergence with an upward flow at low level.

This meridional teleconnection occurs at 500 and 850-hPa (Fig. 2b, c), suggesting its quasi-barotropic structure. Convergence of flow over SEC at 850 hPa leads to increased rainfall. Additionally, notably, the abnormal cyclone at 850-hPa in the Philippines, together with the positive vorticity anomaly, could lead to more precipitation over SEC through the Pacific-Japan teleconnection pattern

Fig. 2 Differences in the wind vector, 1961–2001. The wind vector represents the difference between the years with more and less precipitation in SEC (in the *blue rectangle*). **a** 200-hPa, **b** 500-hPa and **c** 850-hPa. The *shaded* areas represent to the 95 % confidence level (color figure online)
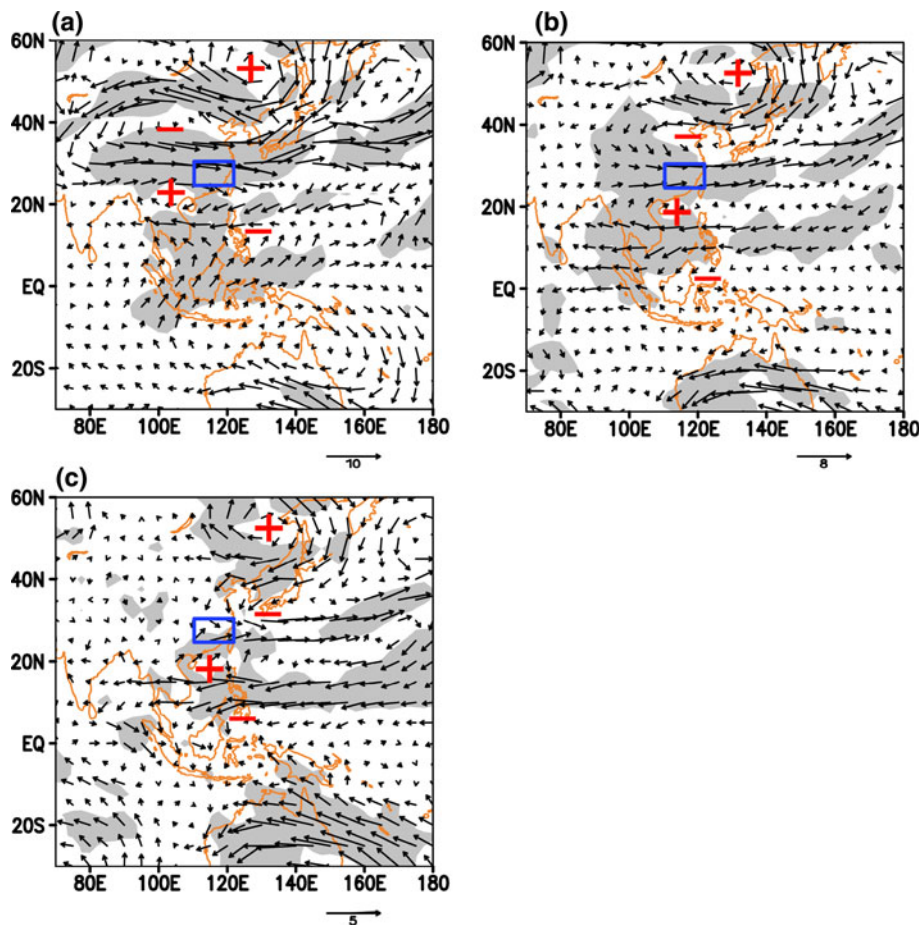
(Nitta 1987; Huang and Li 1987). The 200-hPa geopotential height over the Tibetan Plateau and the 850-hPa vorticity near Philippines are selected as two predictors.

3.2 The SST in winter

Precipitation over China is affected by the internal dynamics of the monsoonal circulation and external forcing (Webster et al. 1998). The SST is usually regarded as an important predictor of seasonal climate because of its long-term sustainability with respect to atmospheric processes. The SST in key regions influences atmospheric circulation, such as the summer monsoon, and affects rainfall or other weather processes (Namias 1969; Namias and Cayan 1981; Ratcliffe and Murray 1970). The corresponding anomalous monsoonal flow through the Western Pacific Subtropical High affects the direction and strength of the water vapor transport into eastern China (Huang and Lu 1989; Wu et al. 2003; Zhou and Yu 2005), leading to the interannual variability in precipitation. The Kuroshio Current is one of the strongest western-boundary currents in the warm pool. It acts as a heat source, producing long-term weather anomalies (Gu et al. 2004) that affect summer rainfall over SEC (Chen and Qian 2005; Zhang et al. 1998). The SST in the central and eastern tropical Pacific is dominated by ENSO, and the ENSO signal has been regarded as a key predictor of summer precipitation over China (Huang and Wu 1987; Jian et al. 2006; Wu et al. 2009b).

Further analysis of the correlation between the global SST from the preceding winter and the SEC area-averaged summer rainfall as a year-to-year increment is carried out to investigate the delaying influences of the SST on summer rainfall over SEC during 1961–2001(Fig. 3). The 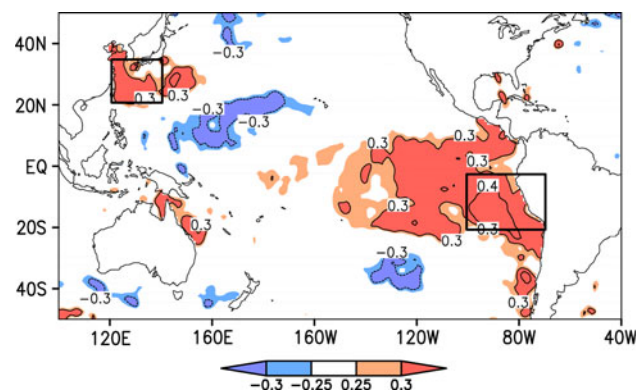patterns in the correlation coefficients (CCs) indicate that the regions 20.5°–34.5°N, 120.5°–140.5°E and 19.5°–2.5°S, 105.5°–70.5°W had the most significant positive correlation during the preceding winter (Wu et al. 2009a). Consequently, the winter year-to-year increments in the SST in the above two regions are chosen as predictors.

3.3 The SLP in May

Cold-dry and warm-moist flows are primary requirements of precipitation. The CCs between the SEC area-averaged summer rainfall and the SLP in May as a year-to-year increment indicate that significant positive and negative correlations are found in central Siberia and Northeast China, respectively (figure not shown). This pattern could lead to a longitudinal pressure gradient, which would support the southward advection of cold air to SEC. This scenario closely resembles that outlined by Samel et al. (1999). Thus, the year-to-year increment in the SLP (over 40°–50°N, 90°–110°E) in May is selected as another key dynamic predictor for summer rainfall over SEC.

3.4 200-hPa divergence in summer

The correlation coefficient between area-averaged summer rainfall over SEC and the 200-hPa divergence as a year-to-year increment are given in Fig. 4. The significant negative correlations are seen in the region of 10°–20°N, 110°–150°E (see Fig. 4), in which circulation is one of important components of the Monsoon-El Niño-Southern Oscillation system (Kleeman et al. 1999). It is known from the previous analysis that an abnormal cyclonic circulation is also located in this region (10°–20°N, 110°–150°E) (Fig. 2a) (Wu et al. 2009b). Figures 4 and 2a suggest that the
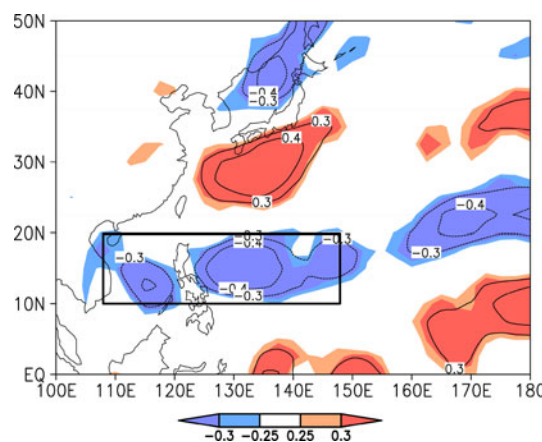

Fig. 3 The correlation coefficients between area-averaged summer rainfall over SEC and the SST from the previous winter, expressed as year-to-year increments. The *shaded* areas from *light* to *dark* colors correspond to the 90 and 95 % confidence levels, respectively, and the rectangles represent the chosen domains where the predictors SST_{KU} and SST_{SP} are defined (color figure online)

Fig. 4 The correlation coefficients between area-averaged summer rainfall over SEC and summer divergence at 200-hPa as year-to-year increments from 1961 to 2001. The *shaded* areas from *light* to *dark* colors correspond to the 90 and 95 % confidence level, respectively, and the rectangles indicate the region selected to define the predictor Div_{200WTP} (color figure online)

abnormal circulation system in 10°–20°N, 110°–150°E could cause more rainfall over SEC. Therefore, the 200-hPa divergence over 10°–20°N, 110°–150°E, should be recognized as a predictor.

3.5 East Asian monsoon index and Western Pacific subtropical high in summer

The interannual variability in the East Asian summer monsoon can influence droughts and floods in China (Ding 1992; Tao and Chen 1987). Usually, an enhanced EASM leads to more rainfall over northern China and less rainfall over southern China. The correlation coefficient between EASMI and the area-averaged SEC is 0.47 (Table 1). In addition, the Western Pacific subtropical high is one of important components of East Asian summer monsoon system; its seasonal variations in intensity, structure, and location can influence the distribution of summer rainfall in eastern China (Tao and Xu 1962; Huang 1963; Tao and Chen 1987; Ding 1994).Therefore, we chose the year-to-year increment in summer EAMI and 500-hPa geopotential height over SEC as predictors.

3.6 850-hPa specific humidity in summer

Rainfall is strongly related to atmospheric moisture. Plenty of water vapor is transported to the East Asian monsoon region by large-scale atmospheric circulations from the adjacent oceans (Zhou and Yu 2005). South Indian ocean is a major source of water vapor, and the Somali Jet brings water vapor from the Southern Hemisphere to the Northern Hemisphere during the boreal summer (Wang and Xue 2003; Ding 2005). Therefore, the year-to-year increment in 850-hPa specific humidity (q_{850}) over 20°–10°S, 70°–100°E in the summers of 1961–2001, is selected as predictors.

Based on the above analysis, nine year-to-year increment predictors are established according to their physical linkages with SEC summer rainfall (5th column of Table 1). The SST_{KU} and SST_{SP} in winter represent the effect of the Pacific warm pool and ENSO, respectively; the SLP_{MG} in May represents the cold-air activity at high latitudes; the summer EAMI represents the strength of the East Asian summer monsoon; the summer Z_{200TIB} is related to the South Asian High; Z_{500SEC} is related to the Western Pacific Subtropical High; the Div_{200WTP} and ζ_{850PI} over the tropical Pacific Ocean in summer are related to the ENSO-monsoon system; and the summer q_{850SIO} represents the water–vapor transport from the Indian Ocean.

As summer predictors are derived from the DEMETER GCM outputs (Table 1), the validity of the DEMETER GCM hindcast should be tested in this context. Table 3 presents the CCs of predictors between the reanalysis data

Table 3 Correlation coefficients of summer predictors as year-to-year increments between the reanalysis data and the DEMETER GCMs during the period 1961–2001

GCMs	EAMI	Z_{200TIB}	Z_{500SEC}	q_{850SIO}	Div_{200WTP}	ζ_{850PI}
CNRM	0.50	0.59	0.52	0.48	0.26	0.66
ECMWF	0.58	0.59	0.58	0.47	0.65	0.69
UKMO	0.55	0.50	0.54	0.45	0.64	0.63

The underlined CCs are above the 99 % confidence level

and the DEMETER GCMs as year-to-year increments. All CCs of the six predictors from the DEMETER GCMs are much greater than 0.40 (99 % confidence level), except for the CCs of Div_{200WTP} for CNRM (0.26, >90 % confidence level). Therefore, the variables from these three DEMETER GCMs are employed in the downscaling model.

4 Results

A statistical downscaling scheme for summer rainfall at each station in SEC is established using multi-linear regression; the model includes nine predictors, and both the predictors and the predictand are represented as year-to-year increments. Two test programs are carried out to validate the predictive capacity. One is an independent sample test: the fitting equations based on each 30 years moving window from 1991 (1961–1990) to 2001 (1971–2000), and this prediction procedure is repeated 11 times during the period 1991–2001. To avoid overfitting in this downscaling scheme, another validation program called a 1-year-out cross-validation is employed, in which any individual year out of 1961–2001 should be the target year among 41 years while the multi-linear regression scheme is established on the remaining 40 years.

4.1 1991–2001 independent sample effect test

To validate the prediction capability of the downscaling scheme, we compared the result based on the downscaling with those from original DEMETER GCM outputs in the form of the year-to-year increment and the total precipitation. Figure 5 shows the interannual variability of spatial ACCs in year-to-year increment form in both the fitting and independent test period. During the fitting period, the spatial ACCs for CNRM, ECMWF, UKMO and MME are greater than the prediction from the original DEMETER GCMs for most years. The multi-year-averaged spatial ACCs of downscaling are increased to 0.66, 0.67, 0.69 and 0.71 for CNRM, ECMWF, UKMO and MME, however, as the original outputs are 0.05, 0.02, 0.08 and 0.03, respectively, for the period 1961–1990 (Fig. 5a). After downscaling, almost all spatial ACCs are greater than 0.25

(95 % confidence level) for all DEMETER GCMs from the period 1961–1990, but not for the original DEMETER GCM results. In the independent test period (1991–2001), the spatial ACCs of downscaling for all DEMETER GCMs are greater than the original results in more than 72 % of the downscaling years (Fig. 5b shown).

The ACCs are also tested for the total precipitation (Fig. 6). For the training period, the largest ACCs of

Fig. 5 Anomaly correlation coefficients (ACCs) of increment of precipitation between observation and original DEMETER GCM or downscaling scheme outputs from the periods 1961–1990 (a) and 1991–2001 (b), respectively. The *horizontal solid line* represents the ACCs at the 95 % confidence level. AVE_B, AVE_F and AVE_T represent the multi-year average ACCs of the original DEMETER GCMs, with downscaling during the periods 1961–1990 and 1991–2001, respectively
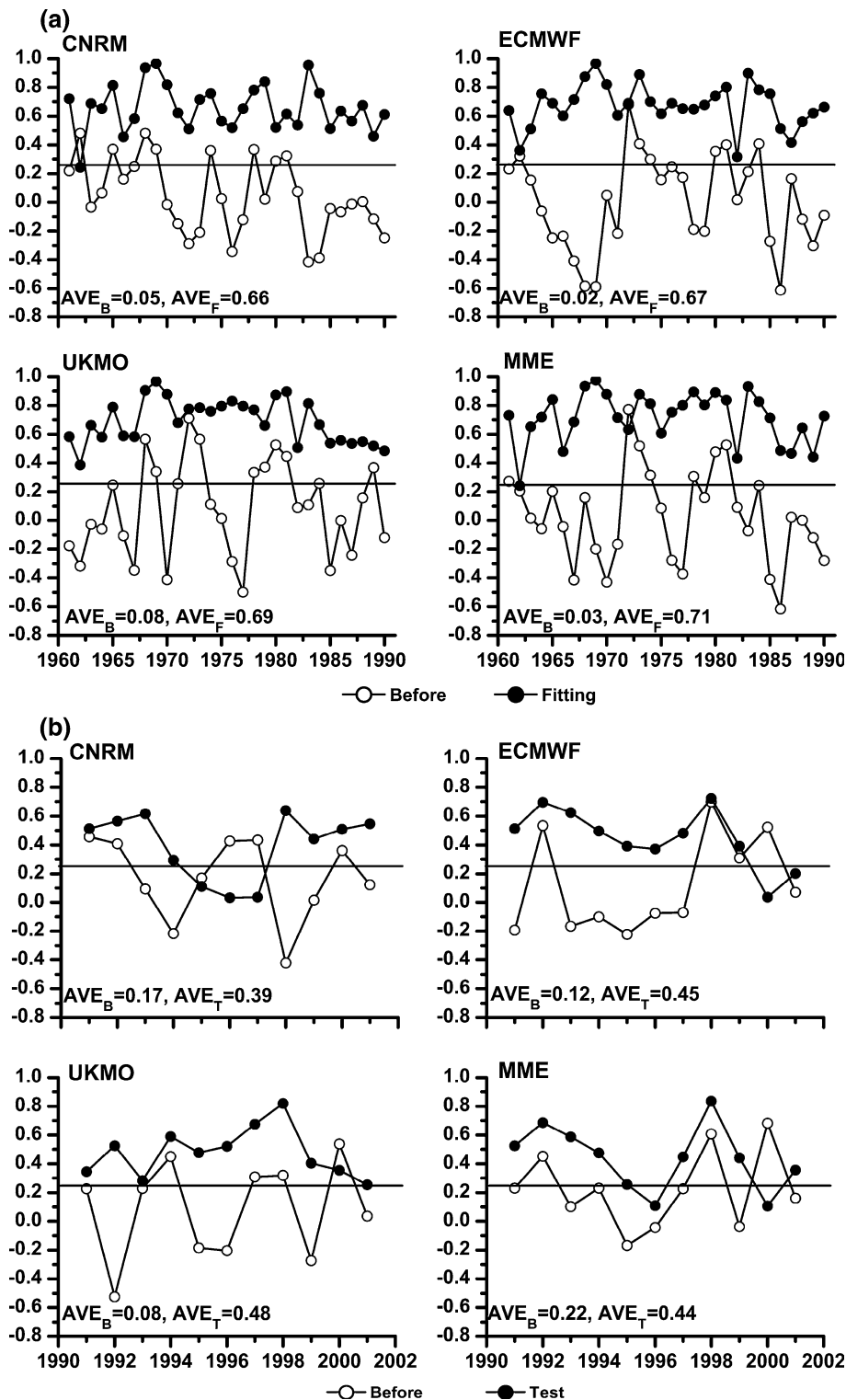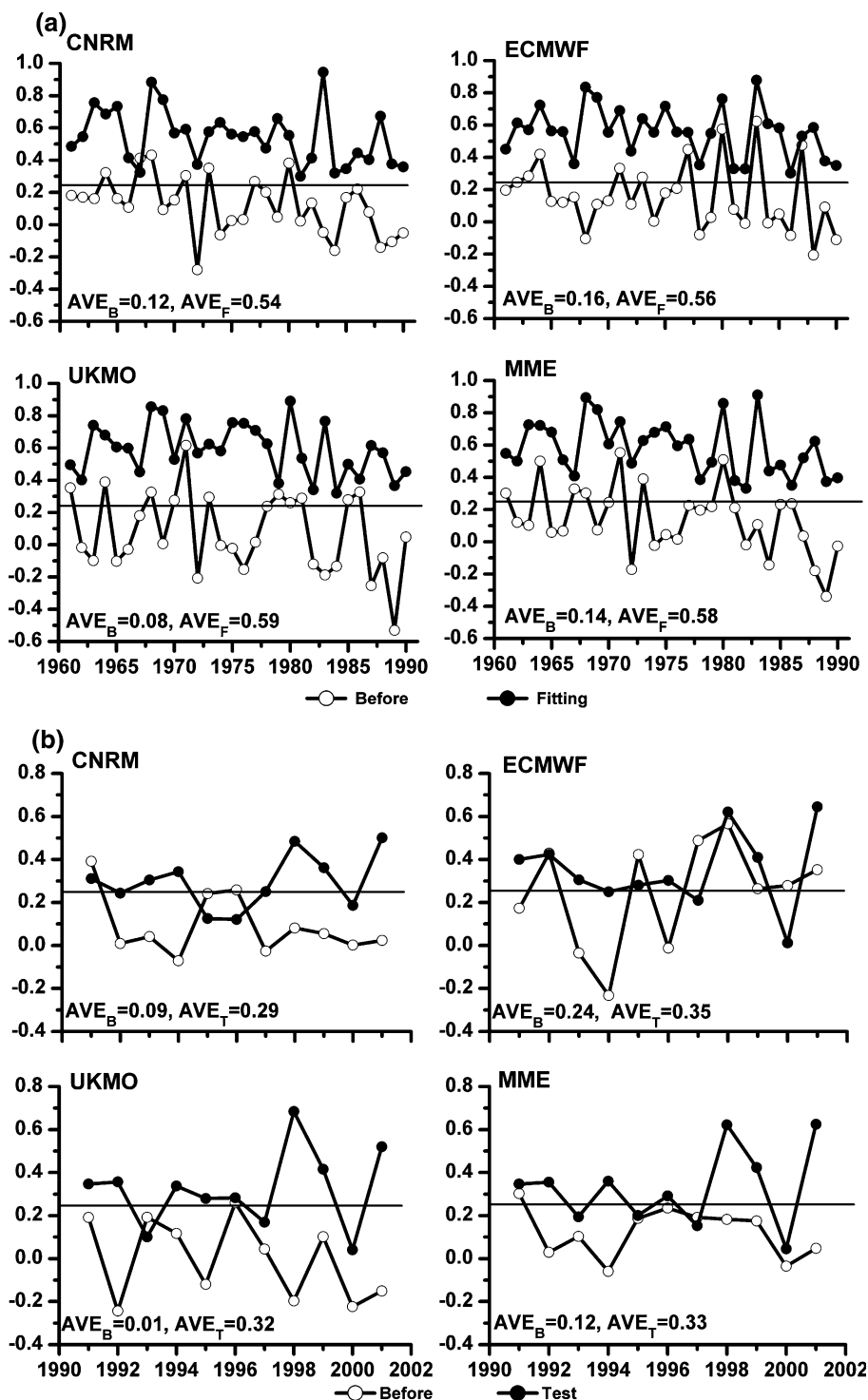
Fig. 6 The same as Fig. 5 but for the total precipitation

downscaled results reach 0.95, 0.88, 0.77 and 0.91, versus, respectively, the values of 0.43, 0.62, 0.62 and 0.55 for the original DEMETER GCMs. The ACCs of downscaling for all DEMETER GCMs are greater than the original results in more than 63 % years during 1991–2001(Fig. 6b shown). For the total precipitation, the downscaled multi-year-average spatial ACCs are 41 % greater than the original DEMETER GCMs for the period 1991–2001. According to the ACCs, the results in the form of the year-to-year increment are greater than the total precipitation from downscaling during the fitting and independent periods.

The $RMSE_{Per}$ is calculated to judge the improvement in predictive skill in RMSE [as shown by formula (4)]. The

Fig. 7 Spatial distribution of $RMSE_{Per}$ for the total precipitation during the period 1991–2001. P represents $RMSE_{Per}$
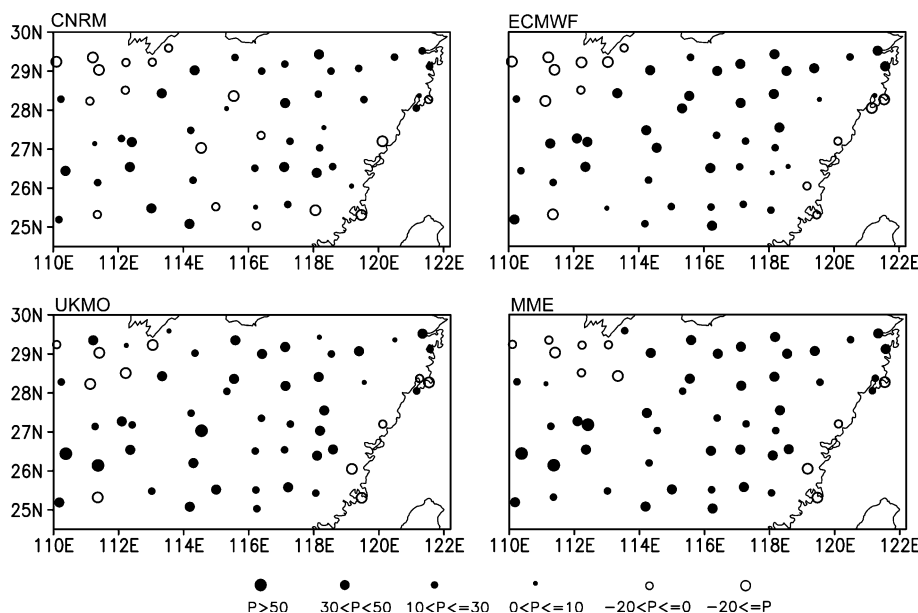

Fig. 8 Anomaly correlation coefficients (ACCs) of increment of precipitation between observation and original DEMETER GCM outputs or downscaling scheme from the period 1961–2001. The *horizontal solid line* represents the ACCs at the 95 % confidence level. AVE_B, AVE_C represents the multi-year-average ACCs of the original DEMETER GCMs and downscaling, respectively
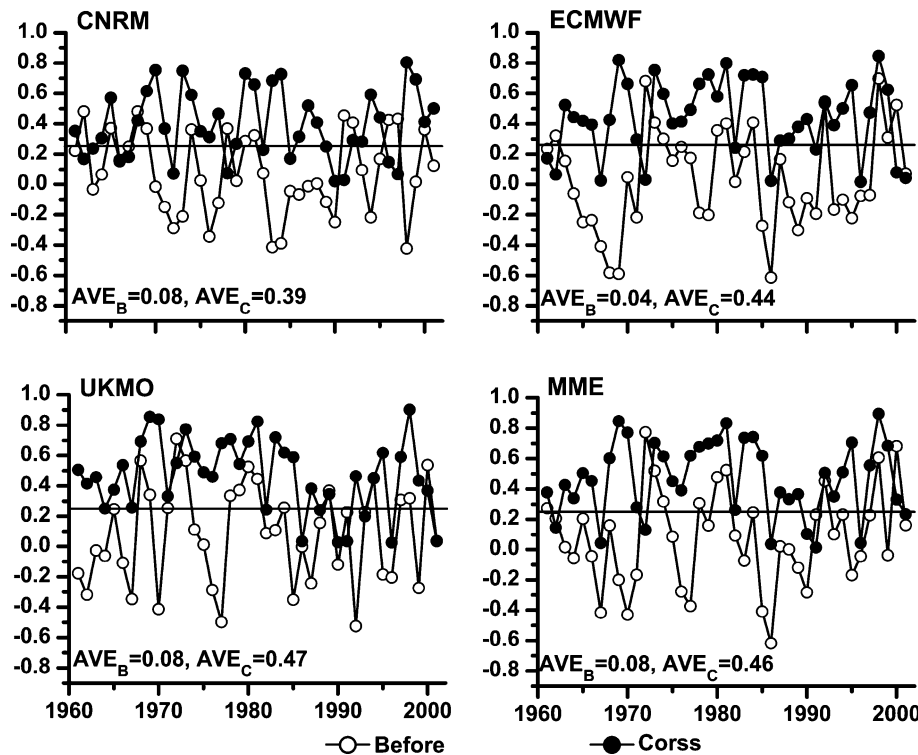
multi-year-averages of the spatial $RMSE_{Per}$ are 8.78, 10.10, 32.70 and 16.70 % for CNRM, ECMWF, UKMO and MME, respectively, for the training period 1961–1990. From 1991 to 2001, the multi-year-averages of the spatial $RMSE_{Per}$ are all greater than zero: 4.34, 6.32, 10.64 and 10.86 % for CNRM, ECMWF, UKMO and MME, respectively. Clearly, the $RMSE_{Per}$ values are greater than zero in more than 66 % years (figures not shown).

The spatial pattern of $RMSE_{Per}$ in relation to the total precipitation is also examined. The $RMSE_{Per}$ distribution of CNRM, ECMWF, UKMO and MME at 57 stations is given in Fig. 7. Analysis reveals that $RMSE_{Per}$ values are positive for all DEMETER GCMs in SEC, except in the northwestern part of SEC and other individual stations. Therefore, the improvement in $RMSE_{Per}$ is also highly significant in the independent test period (1991–2001).

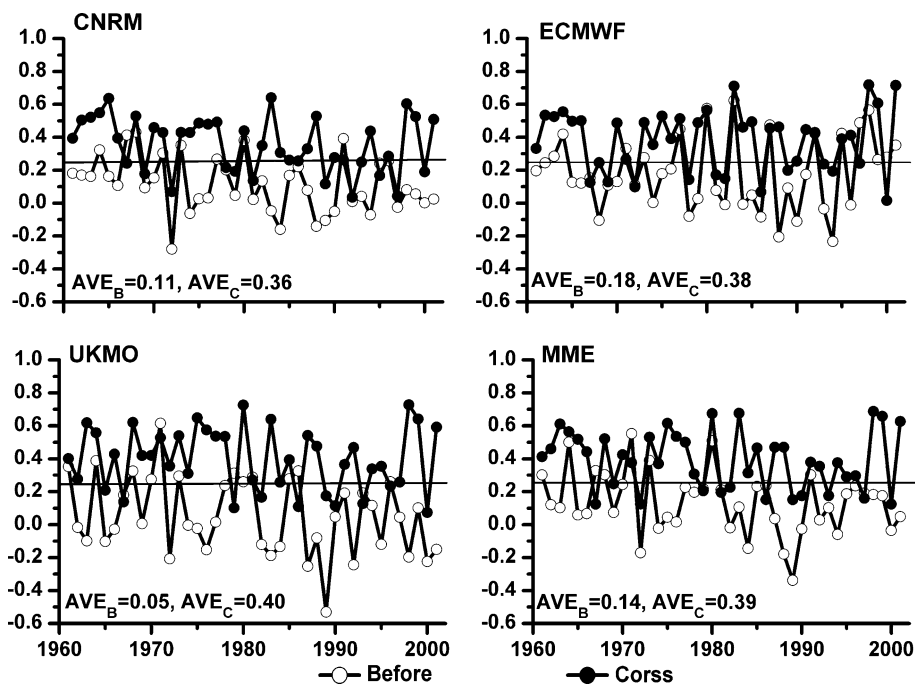**Fig. 9** The same as Fig. 8, but for the total precipitation

Fig. 10 Spatial pattern of the time correlation coefficients (TCCs) of increment of precipitation between the observation and the original DEMETER GCM outputs or downscaling scheme results from 1961 to 2001. CNRM-B and CNRM-C presented the TCCs between the observation and the original DEMETER GCMs and the downscaling scheme outputs, respectively, like the other GCMs. The *light and dark shaded* areas represented the 90 and 95 % confidence levels, respectively
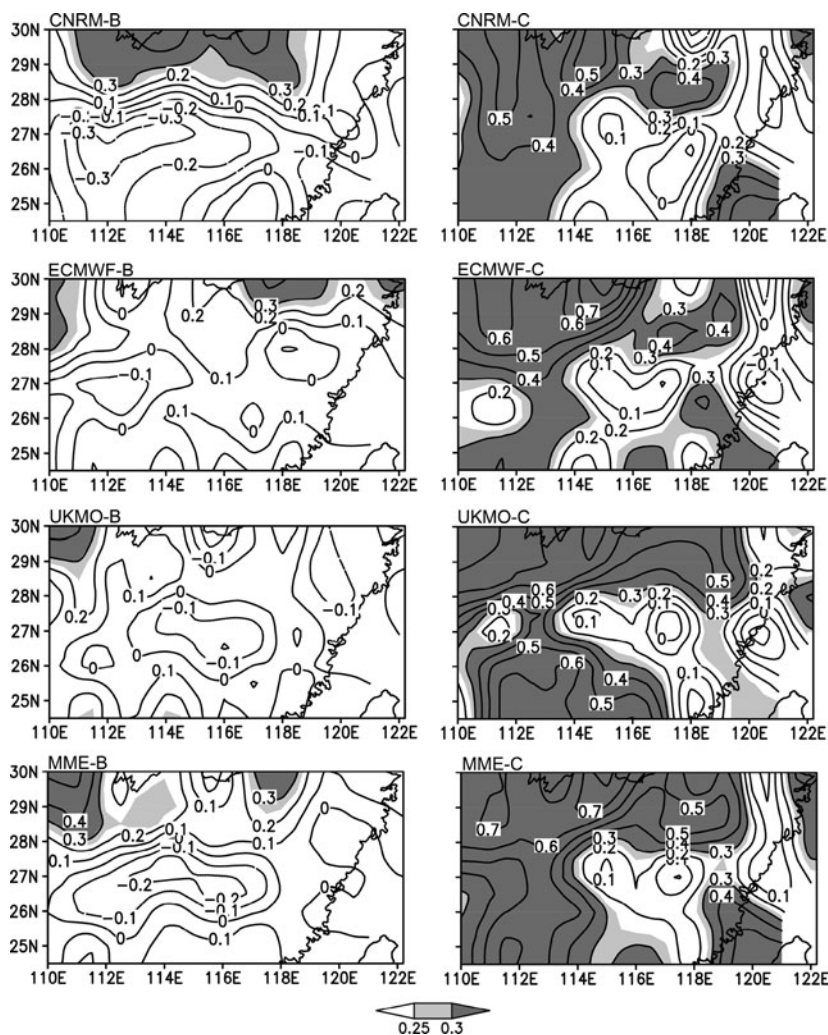
4.2 1961–2001 cross-validation

To interpret the stability of the downscaling method, we also carried out a 1-year-out cross-validation (Michaelsen 1987) from 1961 to 2001. The downscaled multi-year-average spatial ACCs as the year-to-year increments based on CNRM, ECMWF, UKMO and MME are 0.39, 0.44, 0.47 and 0.46 versus 0.08, 0.04, 0.08 and 0.08 for the original DEMETER GCM outputs, respectively (Fig. 8). On the other hand, the downscaled multi-year-average spatial ACCs for the total precipitation based on CNRM, ECMWF, UKMO and MME are approximately 0.36–0.40 compared with approximately 0.05–0.18 for the original DEMETER GCM outputs, respectively (Fig. 9). The spatial ACCs of downscaling are larger than original results in

more than 78 % years during the period 1961–2001 on the year-to-year increment and total precipitation. In addition, the multi-year-averaged spatial ACCs of the total precipitation in cross-validation are considerably better than those in the independent sample test. In more than 25 % of the downscaling years, the spatial $RMSE_{Per}$ are greater than zero. In particular, the 41-year averages of spatial $RMSE_{Per}$ are 4.87, 6.95, 13.37 and 12.99 % for CNRM, ECMWF, UKMO and MME, respectively.

The 41-year temporal correlation coefficients (TCCs) are given in Fig. 10 as the year-to-year increments in the downscaled rainfall based on comparisons between the model-predicted and original DEMETER GCM outputs and the observed counterpart data. Overall, the TCCs of downscaling, which are significant over most parts of SEC,

Fig. 11 The same as Fig. 10, but for the total precipitation
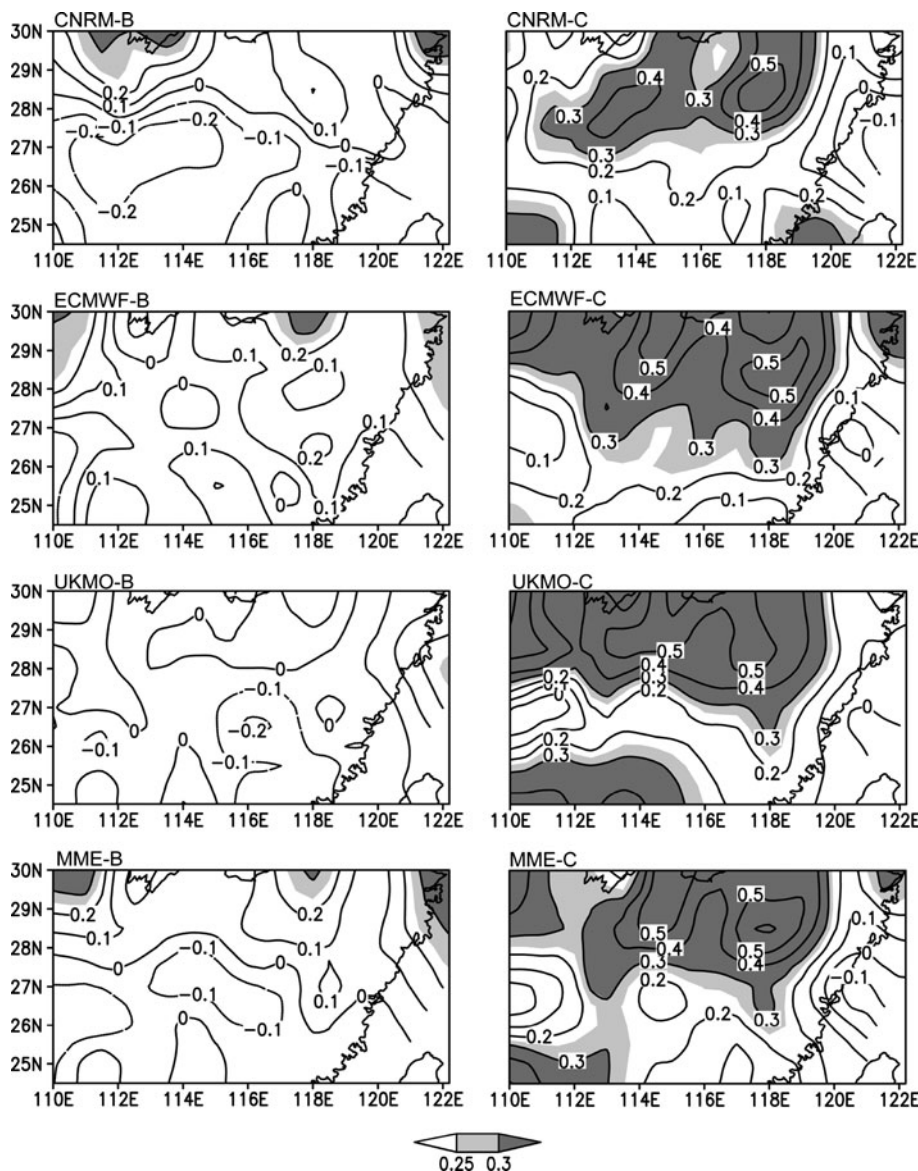
are greater (approximately 0.2–0.7) than those of original outputs (<0.2). The left column of Fig. 10 shows that all original DEMETER GCMs have almost no predicted skill for summer rainfall in the form of year-to-year increments over SEC, and the TCCs over most parts of SEC are no greater than 0.25 (90 % confidence level) even negative in central SEC.

Figure 11 shows the TCCs for the total precipitation. Compared with the hindcast from the original DEMETER GCMs, the TCCs of statistical downscaling over SEC also increase significantly for all DEMETER GCMs, especially in the central and northern regions (the right column of Fig. 11). The spatial pattern of RMSE$_{Per}$ for the total precipitation is also analyzed in the cross-validation (Fig. 12); after downscaling, positive RMSE$_{Per}$ are found in most of stations in SEC for all DEMETER GCMs and MME, indicating considerable improved predicted skill.

5 Conclusion and discussion

In this study, working from the year-to-year increments in summer rainfall at each station in SEC, we develop a hybrid statistical downscaling scheme using both preceding observational information and synchronous hindcasts of DEMETER GCM. Every predictor has a physical linkage to SEC summer rainfall and a significant correlation with SEC (Table 1). Six predictors are derived from DEMETER GCMs, while three from observational data.

Compared with the original DEMETER GCMs prediction, the downscaling scheme can predict the summer rainfall over SEC well in the form of the year-to-year increment and total precipitation. The predicted skill of the year-to-year increment is greater than that of the total

precipitation because the downscaling scheme is based on the predictors and predictand in year-to-year increments. An independent sample test and a cross-validation test are used to validate the predictive skill for summer rainfall both as year-to-year increments and in the original form at each station in SEC. In the independent sample test (during the period 1991–2001), the multi-year-average spatial ACCs of total precipitation are 0.29–0.35, significantly higher than the original DEMETER GCMs results (0.01–0.24). According to the cross-validation in the period 1961–2001, the multi-year-average spatial ACCs of total precipitation also increased by more than 110 % compared with the hindcasts from the original DEMETER GCMs. In addition, the spatial and temporal RMSE are decreased significantly across SEC.

It should also be noted that if three previous predictors derived from observational data (i.e., the SST over the tropical Pacific Ocean and Ocean Kuroshio in the previous winter or the SLP over Mongolia in May) are excluded from this statistical downscaling scheme, the predicted skill is less than that of the downscaled results based on nine predictors (Table 4). Therefore, it is necessary to improve the downscaling predicted skill for SEC summer

Table 4 Comparison of anomaly correlation coefficients from two downscaling prediction schemes

	CNRM	ECMWF	UKMO	MME
Scheme (GCM outputs and observation)	0.36	0.38	0.40	0.39
Scheme (Only GCM outputs)	0.26	0.30	0.31	0.30

One contains nine predictors (chosen from observational data and DEMETER GCM outputs); the other contains six predictors (chosen from DEMETER GCM outputs)

Fig. 12 The same as Fig. 7, but for the cross-validation
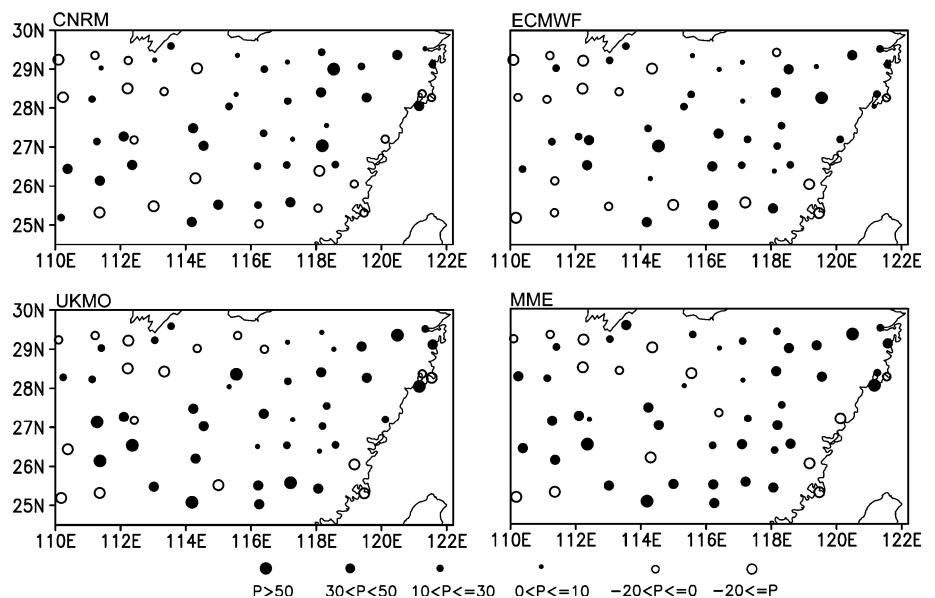
precipitation at each station by including the precursor signal of the observations or an effective dynamical-statistical model.

These results suggested that this downscaling scheme has the potential to improve the predicted skill of summer precipitation in most stations across SEC. Two factors can contribute to improving the predicted skill of downscaling. First, DEMETER GCMs can predict reasonably summer atmosphere circulations related to summer rainfall, although they have no predicted skill at the station level or for localized summer rainfall (Murphy 1999; Zorita and von Storch 1999). Second, the nine predictors in the downscaling prediction scheme contain previous atmospheric/oceanic observational information.

References

Chen YM, Qian YF (2005) Numerical study of influence of the SSTA in western Pacific warm pool on rainfall in the first flood period in South China. J Tropical Meteor 11(1):13–23 (in Chinese)

Chen TC, Wang SY, Huang WR, Yen MC (2004) Variation of the East Asian summer monsoon rainfall. J Clim 17:744–762

Ding YH (1992) Summer monsoon rainfalls in China. J Meteorol Soc Jpn 70:373–396

Ding YH (1994) The summer monsoon in East Asia. Monsoons over China. Kluwer, Dordrecht, pp 1–9

Ding YH (2005) Advanced synoptic meteorology. Meteor Press, Beijing, p 585 (in Chinese)

Fan K (2010) A prediction model for Atlantic named storm frequency using a year-by-year increment approach. Wea Forecasting 25(6):1842–1851

Fan K, Wang HJ (2009) A new approach to forecasting typhoon frequency over the western North Pacific. Wea Forecasting 24:974–986

Fan K, Wang HJ, CHOI YJ (2008) A physically-based statistical forecast model for the middle-lower reaches of the Yangtze River Valley summer rainfall. Chin Sci Bull 53:602–609

Fan K, Lin MJ, Gao YZ (2009) Forecasting the summer rainfall in North China using the year-to-year increment approach. Sci China Ser D Earth Sci 52:532–539

Gao XJ, Zhao ZC, Ding YH, Huang RH, Giorgi F (2001) Climate change due to greenhouse effects in China as simulated by a regional climate model. Adv Atmos Sci 18(6):1224–1230

Gao XJ, Xu Y, Zhao ZC, Pal JS, Giorgi F (2006) On the role of resolution and topography in the simulation of East Asia precipitation. Theor Appl Climatol 86:173–185. doi:10.1007/s00704-005-0214-4

Gao XJ, Shi Y, Zhang DF, Wu J, Giorgi F, Ji ZM, Wang YG (2012) Uncertainties of monsoon precipitation projection over China: results from two high resolution RCM simulations. Clim Res 52:213–226. doi:10.3354/cr01084

Gu DJ, Wang DX, Yuan JN (2004) Anomalous transport of Kuroshion and its relationship with large scale atmosphere-sea interaction. J Torpical Oceanogr 23(6):30–39 (in Chinese)

Huang SS (1963) Longitudinal movement of the subtropical anticyclone and its prediction. Acta Meteor Sin 33:320–332 (in Chinese)

Huang RH, Li WJ (1987) Influence of the heat source anomaly over the western tropical Pacific on the subtropical high over East Asia. In: Proc. International conference on the general circulation of East Asia, 40–51

Huang RH, Lu L (1989) Numerical simulation of the relationship between the anomaly of subtropical high in East Asia and the convective activities in the tropical western Pacific. Adv Atmos Sci 6:202–214

Huang RH, Wu YF (1987) The influence of the ENSO on the summer climate in China and its mechanism[C]. In: Proceedings of Japan–US, Workshop on the El Nino Southern Oscillation Phenomenon. Tokyo University, Tokyo, p 10–15

Jian MQ, Luo HB, Qiao YT (2006) Linkage between the interannual variation patterns of seasonal SST in Indian Ocean–Pacific and their relationship with the summer rainfall over China. J Tropical Meteor 22(2):131–137 (in Chinese)

Ke ZJ, Zhang PQ, Dong WJ, Wang J (2009) An application of optimal subset regression in seasonal climate prediction. Chin J Atmos Sci 33(5):994–1002 (in Chinese)

Kleeman R, McCreary JP Jr, Klinger BA (1999) A mechanism for generating ENSO decadal variability. Geophys Res Lett 26(12): 1743–1746

Lang XM (2011) An effective approach for improving the real-time prediction of summer rainfall over China. Atmos Oceanic Sci Lett 4(2):75–80

Lang XM, Wang HJ (2010) Improving extraseasonal summer rainfall prediction by merging information from GCMs and observations. Wea Forecasting 25:1263–1274

Lang XM, Zheng F (2011) A statistical–dynamical scheme for the extraseasonal rediction of summer rainfall for 160 observation stations across China. Adv Atmos Sci 28(6):1291–1300

Li CY, Sun SQ, Mu MQ (2001) Origin of the TBO-interaction between anomalous East-Asian winter monsoon and Enso cycle. Adv Atmos Sci 18(4):554–566

Liu Y, Fan K, Wang HJ (2011) Statistical downscaling prediction of summer precipitation in southeastern China. Atmos Oceanic Sci Lett 4(3):173–180

Meehl GA (1996) The south Asian monsoon and the tropospheric biennial oscillation. J Clim 10:1921–1943

Meehl GA, Arblaster JM (2002) The tropospheric biennial oscillation and Asian–Australian monsoon rainfall. J Clim 15:722–744

Michaelsen J (1987) Cross-validation in statistical climate forecast models. J Appl Meteor Sci 26(11):1589–1600

Mooley DA, Parthasarathy B (1984) Fluctuations in all-India summer monsoon rainfall during 1871–1978. Clim Change 6:287–301

Murphy J (1999) An evaluation of statistical and dynamical techniques for downscaling local climate. J Clim 12:2256–2284

Namias J (1969) Seasonal interactions between the North Pacific ocean and the atmosphere during the 1960's. Mon Wea Rev 97(3):173–192

Namias J, Cayan DR (1981) Large-scale air-sea interactions and short-period climatic fluctuations. Science 214(4523):869–876

Nitta T (1987) Convective activities in the tropical western Pacific and their impact on the Northern hemisphere summer circulation. J Meteorol Soc Jpn 65:373–390

Palmer TN et al (2004) Development of a European multimodel ensemble system for seasonal-to-interannual prediction (DEMETER). Bull Amer Meteor Soc 85:853–872

Ratcliffe RAS, Murray R (1970) New lag associations between North Atlantic sea temperature and European pressure applied to long-range weather forecasting. Quart J R Met Soc 96(408):226–246

Rayner NA, Parker DE, Horton EB, Folland CK, Alexander LV, Rowell DP, Kent EC, Kaplan A (2003) Global analyses of sea

surface temperature, sea ice, and night marine air temperature since the late nineteenth century. J Geophys Res 108(D14):4407 doi:10.1029/2002JD002670

Samel Arthur N, Wang WC, Liang XZ (1999) The monsoon rainband over China and relationships with the Eurasian circulation. J Clim 12:115–131

Tao SY, Chen L (1987) A review of recent research on the east Asia summer monsoon in China. In: Krishnamurti TN (ed) Monsoon Meteorology. Oxford University Press, New York, pp 60–92

Tao SY, Xu SY (1962) Circulation characteristics in association with persistent summer drought and flood in the Yangtze-Huaihe River reaches. Acta Meteor Sin 32:1–18

Uppala SM et al (2005) The ERA-40 re-analysis. Quart J R Meteor Soc 131:2961–3012. doi:10.1256/qj.04.176

Wang HJ (2000) The interannual variability of the East Asian monsoon and its relationship with SST in a coupled atmosphere-ocean-land climate model. Adv Atmos Sci 17(1):31–47

Wang HJ, Xue F (2003) The interannual variability of Somali jet and its influences on the inter-hemispheric water vapor transport and the East Asian summer rainfall. Chin J Geophys 46(1):11–20 (in Chinese)

Wang SW, Zhu JH (2001) A reviews on seasonal prediction. Adv Atmos Sci 18(2):198–207

Wang B, Lee JY, Kang IS, Shukla J et al. (2008) Advance and prospectus of seasonal prediction: assessment of the APCC/CliPAS 14-model ensemble retrospective seasonal prediction (1980–2004), Clim Dyn. doi:10.1007/s00382-008-0460-0

Wang HJ, Zhang Y, Lang XM (2010) On the predictand of short-term climate prediction. Clim Environ Res 15(3):225–228 (in Chinese)

Webster PJ, Magana VO, Palmer TN, Shukla J, Tomas RA, Yanai M, Yasunari T (1998) Monsoons: processes, predictability, and the prospects for prediction. J Geophys Res 103:14451–14510

Wilby RL, Wigley TML (1997) Downscaling general circulation model output: a review of methods and limitations. Prog Phys Geogr 21(4):530–548

Wu R, Hu ZZ, Kirtman BP (2003) Evolution of ENSO-related rainfall anomalies in East Asia. J Clim 16:3741–3757

Wu B et al (2009a) Seasonally evolving dominant interannual variability modes of East Asian climate. J Clim 22:2992–3005

Wu B et al (2009b) Contrast of rainfall-SST relationships in the Western North Pacific between the ENSO-developing and ENSO-decaying summers. J Clim 22:4398–4405

Yasunari T (1990) Impact of Indian monsoon on the coupled atmosphere ocean system in the tropical Pacific. Meteor Atmos Phys 44:29–41

Yeh TC, Yang GJ, Wang XD (1979) The average vertical circulation over the East-Asia and the Pacific area, (I) in summer. Chin J Atmos Sci 3:1–11 (in Chinese)

Zhang YC, Lu XP, Guo LY (1998) The sensitive experiments of effects of SSTA key regions in winter and spring on the summer precipitation in the middle and lower reaches of the Yangtze River. J Meteor Sic 18(2):150–155 (in Chinese)

Zhao ZG (1999) Summertime floods and droughts in China and the associated circulations. Meteor Press, Beijing, p 297. (in Chinese)

Zhao P, Zhou ZJ (2009) An East Asian subtropical summer monsoon index and its relationship to summer rainfall in China. Acta Meteorol Sin 23:18–28

Zhou TJ, Yu RC (2005) Atmospheric water vapor transport associated with typical anomalous summer rainfall patterns in China. J Geophys Res 110:D08104 doi:10.1029/2004JD005413

Zhou TJ, Wu B, Scaife AA, Bronnimann S, Cherchi A, Fereday D, Fischer AM, Folland CK, Jin KE, Kinter J, Knight JR, Kucharski F, Kusunoki S, Lau NC, Li LJ, Nath MJ, Nakaegawa T, Navarra A, Pegion P, Rozanov E, Schubert S, Sporyshev P, Voldoire A, Wen XY, Yoon JH, Zeng N (2009a) The CLIVAR C20C Project: which components of the Asian–Australian monsoon circulation variations are forced and reproducible? Clim Dyn 33:1051–1068. doi:10.1007/s00382-008-0501-8

Zhou TJ, Wu B, Wang B (2009b) How well do atmospheric general circulation models capture the leading modes of the interannual variability of the Asian–Australian monsoon? J Clim 22:1159–1173

Zorita E, von Storch H (1999) The analog method as a simple statistical downscaling technique: comparison with more complicated methods. J Clim 12:2474–2489